Supplementary Online Material

for

Long-lived Electron Emission Reveals Localized Plasmon Modes in Disordered Nanosponge Antennas

Germann Hergert[1], Jan Vogelsang[1], Felix Schwarz[2], Dong Wang[3], Heiko Kollmann[1], Petra Groß[1], Christoph Lienau[1,4*], Erich Runge[2], and Peter Schaaf[3]

[1]*Carl von Ossietzky Universität, Institut für Physik and Center of Interface Science, D-26129 Oldenburg, Germany*

[2]*Technische Universität Ilmenau, Institut für Physik and Institut für Mikro- und Nanotechnologien MacroNano®, D-98693 Ilmenau, Germany*

[3]*Technische Universität Ilmenau, Institut für Mikro- und Nanotechnologien MacroNano® and Institut für Werkstofftechnik, Fachgebiet Werkstoffe der Elektrotechnik, D-98693 Ilmenau, Germany*

[4]*Forschungszentrum Neurosensorik, Carl von Ossietzky Universität, D-26111 Oldenburg, Germany*

*email: christoph.lienau@uni-oldenburg.de

## 1. Generation of few-femtosecond NIR laser pulses
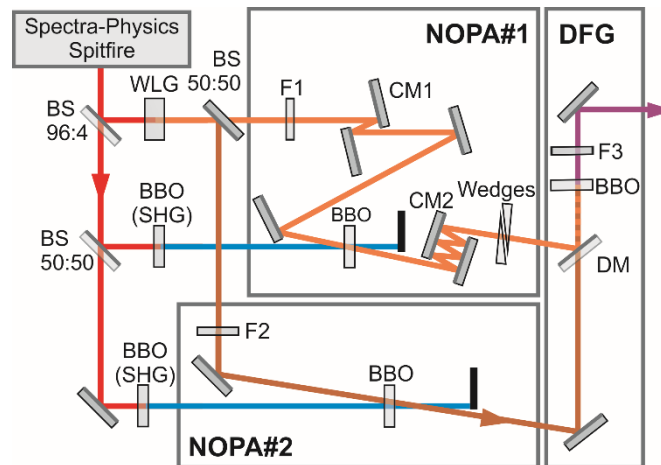
Figure S1. Experimental setup of the laser system. The system is based on pulse generation in two NOPA stages (NOPA#1, NOPA#2), which are seeded by the same white light generation (WLG) source and subsequent difference frequency generation (DFG) of the two pulse trains. Filters F1 and F2 are used to select the spectral ranges for the two NOPA stages. The VIS pulses are compressed before and after NOPA#1 by chirped mirror pairs (CM1 and CM2, respectively). After DFG, residual unwanted frequency components are removed by a long-pass filter (F3) before the vacuum chamber containing the gold nanotip. Reproduced with permission from Ref. 1. Copyright 2014, The Optical Society of America.

In our experiments, few-cycle pulses at a center wavelength of 1600 nm are used to initiate photoemission from gold sponges. Such pulses are derived from a regenerative Ti:Sapphire amplifier (Spectra Physics Spitfire) with a repetition rate of 5 kHz. They are generated in two non-collinear optical parametric amplifier (NOPA) stages, which are seeded by the same white light, followed by difference frequency generation (DFG) between the output pulses from these two NOPA stages to reach the near-infrared (NIR) spectral region.[1]

The first NOPA stage (NOPA#1) supports amplification of a broad spectral range from 530 nm to 640 nm and yields a pulse energy of about 3.6 μJ. The pulses are compressed using chirped mirrors and pulse duration measurements indicate a nearly transform-limited pulse duration of 9 fs.

The seed for the second NOPA stage (NOPA#2) is filtered to a narrow bandwidth of 10 nm, centered at 890 nm. The output pulses of both NOPA stages are spatially and temporally overlapped in a third BBO crystal cut for DFG. With the fixed, narrow-bandwidth output of NOPA#2, the wide bandwidth of NOPA#1 is directly transferred to the NIR by the DFG process. The NOPA-DFG system supplies pulses of up to 110 nJ energy with a bandwidth in excess of 500 nm centered at 1600 nm (Figure S2). After compression, we measure a near-transform limited pulse duration of 16 fs by interferometric frequency-resolved autocorrelation (IFRAC)[2] using frequency doubling in a β-barium borate (BBO) crystal (Figure S2).
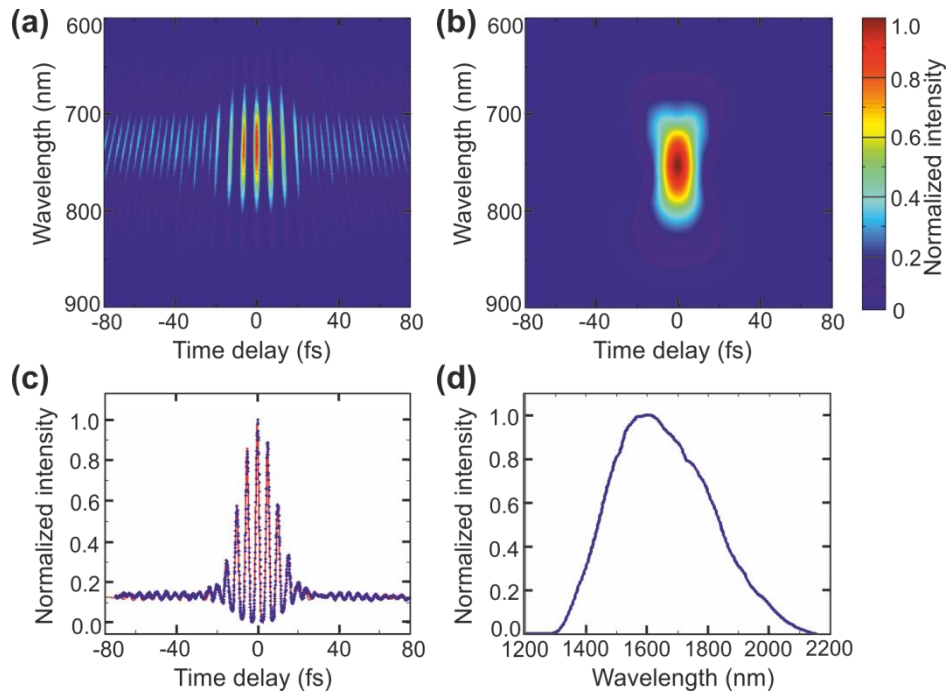
Figure S2. Interferometric autocorrelation of the laser pulses. (a) Interferometric frequency-resolved autocorrelation (IFRAC) of the output pulses of the NOPA-DFG system and (b) simulated frequency-resolved optical gating (FROG) trace using the complex electric field amplitude retrieved from the IFRAC measurement. (c) The interferometric autocorrelation (IAC) calculated from the retrieved electric field amplitude (red curve) and the IAC obtained by projecting the measured IFRAC trace from (a) onto the time delay axis show good agreement. The IAC indicates a pulse duration of 16 fs. (d) The spectrum covers >500 nm, centered at 1600 nm.

Since the two NOPA stages are seeded by the same white light, they inherently share the same carrier-envelope phase (CEP). Thus, by DFG of the two NOPA output pulse trains, the resulting NIR pulses are passively CEP-stabilized.[3,4] We have previously demonstrated a shot-to-shot CEP RMS noise of about 800 mrad as well as an excellent long-term CEP stability of this source of better than 50 mrad over time spans up to 20 minutes, when averaging over 100 pulses.[1]

2. Experimental setup for electron photoemission from nanoporous gold sponges
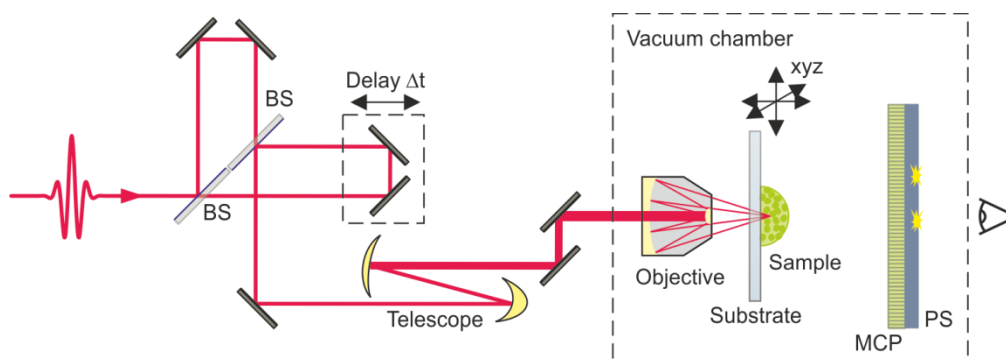
Figure S3. Experimental setup for photoelectron spectroscopy. The light pulses from the NOPA-DFG light source are split into two replicas using a Mach-Zehnder interferometer. The delay between the pulses is adjusted by changing the length of one arm. The beam is focused onto the sample using a Cassegrain objective. Electrons are detected by a multi-channel plate (MCP) followed by a phosphor screen (PS).

The nanoporous gold sponges are illuminated with a sequence of two identical, precisely temporally delayed pulses. The experimental setup is sketched in Figure S3. The two pulse replicas are created in a Mach-Zehnder interferometer by splitting the pulses from the NOPA-DFG source described above using a 50:50 beam splitter (BS). The time delay between the two replicas is adjusted by changing the path length of one interferometer arm before recombining them at a second BS. A 1:2 all-reflective telescope is used to match the beam diameter to a Cassegrain objective with 0.5 numerical aperture (NA). The beam is focused onto the nanoporous gold sponge under investigation through the substrate, which consists of glass coated with a transparent and conductive indium tin oxide (ITO) film. The focus diameter is around 2.8 μm, which is larger than the diameter of a single nanosponge yet sufficiently small to excite only one of the sponges at a time. Electrons that are emitted from the surface of a gold sponge, i. e., on the far side of the sample, are accelerated towards the detector by applying a small voltage of -10 V between sample and detector. The detector consists of a multi-channel plate (MCP), followed by a phosphor screen (PS). The luminescence from the screen induced by electron impact is captured using a camera. The objective, sample, MCP and phosphor screen are mounted inside a vacuum chamber with a base pressure of $<10^{-6}$ mbar.

3. Theoretical model for long-lived hot spot resonances

The presence of long-lived hot spot resonances on the gold nanosponges is experimentally verified, as described in the main manuscript, by performing time-resolved photoemission experiments on single nanosponges. We observe photoemission for delays of more than 50 fs, which is much longer than the pulse duration. This long-lived response function was explained by long-lived and narrow-bandwidth hot spot resonances superimposed on a short-lived and delocalized dipolar resonance of the gold particle. Here we explain the model and the results in increasing steps of complexity. Exemplarily, we compare the model with the experimental results obtained for the nanoporous gold sponge labelled "particle A" in the main text.

A time-dependent electric field $E_L(t)$ that is incident on the nanoporous gold sponge excites a short-lived delocalized plasmon resonance, similar to the plasmon resonance of a solid gold nanoparticle, which is assumed to decay exponentially with a short decay time τ_P. In addition, N hot spot resonances with a longer decay time τ_H are excited. In response to a delta pulse excitation, any of the plasmon resonances will oscillate with the resonance frequency ω_P for the delocalized plasmon and with ω_j for the j-th localized plasmon, with $j = 1, 2 \ldots N$. These oscillations decay exponentially with the time constants τ_P and τ_H, respectively. For simplicity, we have assumed the same lifetime for all localized hot spot plasmon resonances in each simulation. Each localized hot spot plasmon field can interfere with the delocalized plasmon field, creating a superposition of the two oscillating terms, but in our model we have excluded interference of the localized fields of two different hot spots. This is assumed, because the average distance between hot spots is much larger than the extent of the localized near field (compare FDTD simulation shown in Figure 4b in the main text). Hence we first derive electron emission for the field originating from each hot spot in combination with the delocalized plasmon mode, before incoherently adding together the electron contributions from the different hot spots.

At each spot, the short-lived plasmon field couples to the long-lived, and hence spectrally much sharper resonance of the corresponding hot spot. This means they have a sharp resonance that is coupled to a quasi-continuum (the broadband dipolar plasmon resonance), a situation that has first been treated by Fano in the autoionization of Helium atoms.[5] Later, a similar model to describe such Fano-type resonances has also been used in plasmonic crystals[6-8] or systems of coupled metal nanostructures.[9] Then, the local electric field strength on the surface of the sponge at time t and at the position of hot spot j is given by the convolution of the incident field and the local response function, which can be taken as the sum the damped exponentials delocalized and the j-th localized plasmon resonance:

$$E_{S,j}(t) = E_L(t) \otimes \left[\Theta(t) \left(A_P \cdot e^{-i\omega_P t} \cdot e^{-t/\tau_P} + A_j \cdot e^{-i\omega_j t} \cdot e^{-t/\tau_H} \right) \right]. \tag{1}$$

Here, $\Theta(t)$ is the Heaviside function, and A_P and A_j are the relative amplitudes of the delocalized and of the j-th localized plasmon mode, respectively. The response of the individual plasmon resonances to the driving field is implemented in the frequency domain, and the fields $E_{S,j}(t)$ are then reconstructed by an inverse Fourier transform. The incident electric field in the frequency domain is given as

$$\tilde{E}_{\text{L}}(\omega) = \frac{1}{\sqrt{2\pi}} \int_{-\infty}^{\infty} E_{\text{L}}(t) \cdot e^{-i\omega t} \, dt \tag{2}$$

and the response function of the delocalized and the j-th localized plasmon resonance is written as

$$\tilde{R}_{j}(\omega) = \int_{-\infty}^{\infty} \Theta(t) \left(A_{\text{P}} \cdot e^{-i\omega_{\text{P}} t} \cdot e^{-t/\tau_{\text{P}}} + A_{j} \cdot e^{-i\omega_{j} t} \cdot e^{-t/\tau_{\text{H}}} \right) \cdot e^{-i\omega t} \, dt \,. \tag{3}$$

In the frequency domain, the electric field strength of hot spot j is then given by the product

$$\tilde{E}_{\text{S},j}(\omega) = \tilde{E}_{\text{L}}(\omega) \cdot \tilde{R}_{j}(\omega). \tag{4}$$

The resulting temporal field of the j-th hot spot is obtained by performing the inverse Fourier transform of the spectral field $\tilde{E}_{\text{S},j}(\omega)$:

$$E_{\text{S},j}(t) = \frac{1}{\sqrt{2\pi}} \int_{-\infty}^{\infty} \tilde{E}_{\text{S},j}(\omega) \cdot e^{i\omega t} \, d\omega \tag{5}$$

The local field $E_{\text{S},j}(t)$ gives rise to multiphoton electron emission in a nonlinear process of order $2 \cdot n$ of the electric field. From experimental measurements, we obtain the order of nonlinearity $n = 5$, which is employed in our calculations. The temporal dynamics of the oscillating plasmon field is studied experimentally by measuring an interferometric autocorrelation (IAC) trace of the photoemission. This is performed by illuminating the gold sponge by a sequence of two pulses with delay Δt, and by measuring the electron yield $C(\Delta t)$ as a function of delay. In order to compare the numerical model with the experimentally measured IAC, we generate the corresponding function $C(\Delta t)$ numerically. For this we first calculate the IAC $C_{j}(\Delta t)$ for each hot spot as:

$$C_{j}(\Delta t) = \int_{-\infty}^{\infty} \left| \left(E_{\text{S},j}(t) + E_{\text{S},j}(t + \Delta t) \right)^{n} \right|^{2} \, dt \tag{6}$$

Subsequently the different contributions of the hot spots are incoherently added together to yield the total electron count:

$$C(\Delta t) = \sum_{j=1}^{N} C_{j}(\Delta t) \tag{7}$$

The model is implemented using the complex field amplitude that was derived from the IFRAC measurements (see Figure S2) as the incident light field $E_{\text{L}}(t)$. The resonance of the delocalized plasmon mode is centered at $\lambda_{\text{P}} = 1500 \, \text{nm}$, and its decay time is taken as $\tau_{\text{P}} = 5 \, \text{fs}$. We have varied the number of localized hot spots and their resonance frequencies to approximate the measured dark-field spectra and IACs, while we have assumed a constant decay time for all hot spots in one simulation, which is much larger than that of the delocalized plasmon mode.
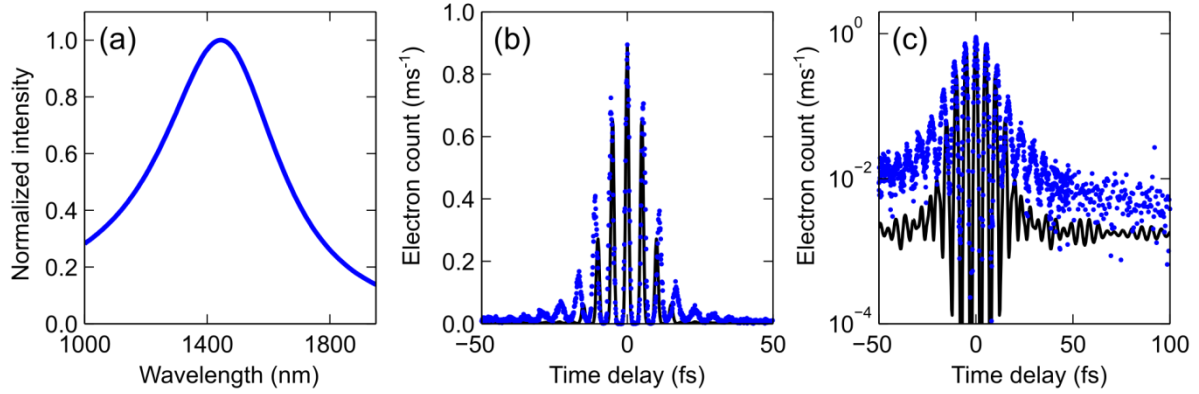
Figure S4. Interferometric autocorrelation trace of photoemission simulated for a single dipolar resonance. (a) Model dark field spectrum of a solid gold particle with only a broad and short-lived resonance. **(b)** Simulated IAC trace (black line) plotted together with the experimental data (blue symbols) on a linear scale. In **(c)** the same simulated and experimental IAC are shown as in (b) but on a logarithmic scale. The resonance as shown in (a) is centered at 1500 nm and has a spectral width of 550 nm, corresponding to a plasmon decay time of 5 fs. A nonlinearity of order 5, matching the experimentally measured value, is assumed. Without long-lived plasmon resonance, the simulated IAC trace cannot account for the persistent electron emission for long delay times.

As a reference example, we calculate IAC traces expected for a (non-porous) solid gold nanoparticle. Such a particle should only show a single broad dipole resonance, which results in a nearly instantaneous response of the particle. For the simulations, we have taken only one resonance centered at $\lambda_P = 1500\,\text{nm}$ and with a fast decay time of $\tau_P = 5\,\text{fs}$ in Eqs. (1) and (3), corresponding to a spectral bandwidth of ~550 nm. This yields the expected broad-bandwidth intensity spectrum shown in Figure S4a. The IAC shows interference fringes only at very short delays, which mainly reflects the convolution of the incident field and the short-lived plasmon response. When assuming a nonlinearity of order 5, the central fringes of the measured curve are well reproduced. The measured IAC photoelectron emission, however, persists over a much longer delay. This shows clearly that this simple model, taking into account only one short-lived (delocalized) plasmon mode, is not sufficient to describe our experimental observations.

In a next step, we show the results of a model taking into account one long-lived hot spot resonance in addition to the short-lived dipolar mode discussed above. For this we have set $N = 1$ and $A_1 = 2 \cdot A_P$. The resonance was centered at $\lambda_1 = 1700\,\text{nm}$ and had a long decay time of $\tau_H = 40\,\text{fs}$. The center wavelength λ_1 was chosen to match the IAC fringe spacing at long delays while the lifetime was adopted to match the overall decay of the fringes. The short-lived delocalized plasmon resonance was kept at $\lambda_P = 1500\,\text{nm}$ and $\tau_P = 5\,\text{fs}$, as before.

6
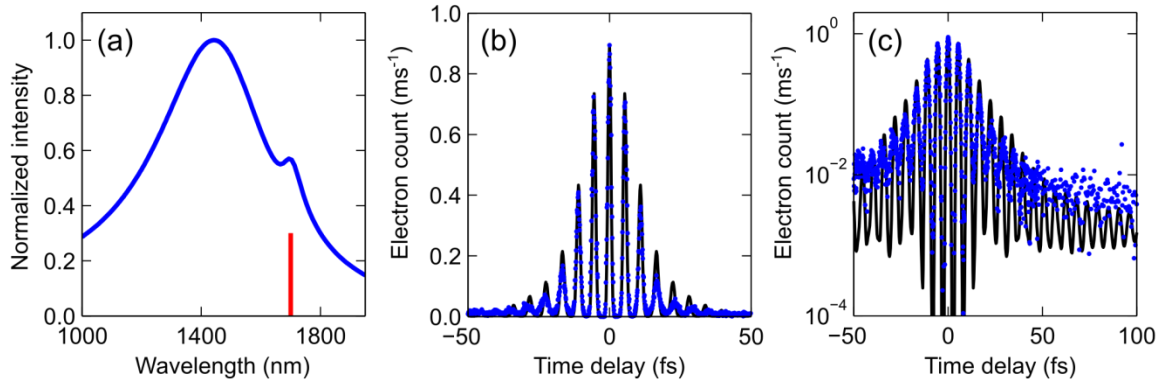
Figure S5. Interferometric autocorrelation modeled for a gold nanosponge with a single hot spot. (a) Model dark field spectrum of the nanosponge with one broad, short-lived resonance and one narrow resonance (blue curve). The red line indicates the position and relative strength of the sharp hot spot resonance. **(b)** Simulated interferometric autocorrelation (IAC) trace (black line) plotted together with the experimental data (blue symbols) on a linear scale. In **(c)** the same simulated and experimental IAC are shown as in (b) but on a logarithmic scale. In this model the persistent emission at long delays is well reproduced but the modulation of each fringe is more pronounced than in the measured IAC.

The intensity spectrum shown in Figure S5a now displays one clear narrow feature on top of the broad spectrum, with a typical, slightly dispersive Fano line shape. The amplitude of this spike is much larger than the modulation on the experimentally measured linear optical spectrum, even if we reduce its peak amplitude by a factor 10^{-4} to account for the small area of the hot spot in comparison with the total surface area of the sponge. Figures S5b and S5c show a strongly modulated interference pattern for long delay times in the simulation. The fringe modulation in the IAC is, however, much more pronounced than measured experimentally. Also, the scattering spectrum (Figure S5a) does not match the experiment since it shows only a single sharp spike. Therefore also this more advanced model cannot account for our experimental observations.
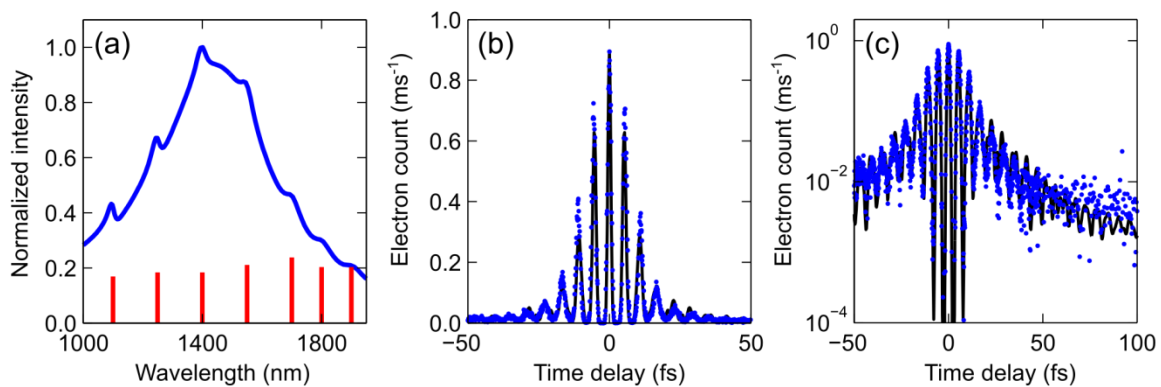
Figure S6. Interferometric autocorrelation modeled for a gold nanosponge with a short-lived dipolar resonance and multiple hot spot resonances. (a) Model dark field spectrum of the nanosponge with a broad, short-lived resonance and seven narrow resonances (blue curve). The colored lines indicate the position and relative strength of the sharp hot spot resonances. **(b)** Simulated interferometric autocorrelation (IAC) trace (black line) plotted together with the experimental data (blue symbols) on a linear scale. In **(c)** the same simulated and experimental IAC are shown as in (b) but on a logarithmic scale. This model yields a good agreement between measured and simulated IACs. (b) and (c) are also shown in the main manuscript as Figure 3d.

We have performed model calculations that led to a rather good agreement with the experiment by assuming photoemission not only from one broad dipole mode but also from multiple hot spot resonances. Their resonance wavelengths have been extracted from the measured linear spectra. Here, seven resonances can be recognized, at wavelengths $\lambda_1 = 1100\,\text{nm}$, $\lambda_2 = 1250\,\text{nm}$, $\lambda_3 = 1400\,\text{nm}$, $\lambda_4 = 1550\,\text{nm}$, $\lambda_5 = 1700\,\text{nm}$, $\lambda_6 = 1800\,\text{nm}$, and $\lambda_7 = 1900\,\text{nm}$. The hot spot amplitudes were chosen such that $\sum A_j = A_\text{P}$, and the relative amplitudes A_j, $j = 1, 2 \ldots 7$ are indicated by the stick spectrum in Figure S6. The lifetime of the plasmon resonances was $\tau_\text{P} = 5\,\text{fs}$ and that of the hot spots was $\tau_j = \tau_\text{H} = 50\,\text{fs}$ for all seven hot spots. We found that we could vary the hot spot lifetime by not more than 10 fs without considerably deteriorating the agreement between measured and simulated IAC. Hence, the corresponding intensity lifetimes of the hot spots is $25 \pm 5\,\text{fs}$. The resulting intensity spectrum in Figure S6a resembles the measured dark-field spectrum in Figure 2 of the main manuscript, and the simulated IAC is indeed acceptable.

References

1. Vogelsang J, Robin J, Piglosiewicz B, Manzoni C, Farinello P *et al*. High passive CEP stability from a few-cycle, tunable NOPA-DFG system for observation of CEP-effects in photoemission. *Opt Express* 2014; **22**: 25295-25306.

2. Amat-Roldán I, Cormack I, Loza-Alvarez P, Gualda E, Artigas D. Ultrashort pulse characterisation with SHG collinear-FROG. *Opt Express* 2004; **12**:1169-1178.

3. Cerullo G, Baltuška A, Mücke OD, Vozzi C. Few-optical-cycle light pulses with passive carrier-envelope phase stabilization. *Laser Photon Rev* 2011; **5**: 323-351.

4. Manzoni C, Cerullo G, De Silvestri S. Ultrabroadband self-phase-stabilized pulses by difference-frequency generation. *Opt Lett* 2004; **29**: 2668-2670.

5. Fano U. Effects of configuration interaction on intensities and phase shifts. *Phys Rev* 1961; **124**:1866-1878.

6. Sarrazin M, Vigneron JP, Vigoureux JM. Role of wood anomalies in optical properties of thin metallic films with a bidimensional array of subwavelength holes. *Phys Rev B* 2003; **67**: 085415.

7. Genet C, van Exter MP, Woerdman JP. Fano-type interpretation of red shifts and red tails in hole array transmission spectra. *Opt Commun* 2003; **225**: 331-336.

8. Ropers C, Park DJ, Stibenz G, Steinmeyer G, Kim J *et al*. Femtosecond light transmission and subradiant damping in plasmonic crystals. *Phys Rev Lett* 2005; **94**: 113901.

9. Luk'yanchuk B, Zheludev NI, Maier SA, Halas NJ, Nordlander P *et al*. The Fano resonance in plasmonic nanostructures and metamaterials. *Nat Mater* 2010; **9**: 707-715.